JOURNAL OF MATERIALS SCIENCE 29 (1994) 5583–5588

# Wetting behaviour and mullite formation at the interface of inviscid melt-spun $CaO–Al_2O_3$ fibre-reinforced Al–Si alloy (4032) composite

YUN-MO SUNG*, KYUNG-YOL YON‡, S. A. DUNN§, J. A. KOUTSKY‡§
*Department of Materials Science and Engineering, ‡Materials Science Program, and §Department of Chemical Engineering, University of Wisconsin-Madison, Madison, WI 53706, USA*

Inviscid melt-spun calcia–alumina fibre-reinforced aluminium–silicon alloy (4032) composites were produced using a melt-infiltration technique. Scanning electron microscopy, energy dispersive X-ray spectroscopy (EDS), and X-ray diffraction (XRD) were used to investigate interfacial wetting and interphase formation, and identify the crystalline phase of the interphase of these composites. The composites processed at 700 °C showed a good interfacial wetting and silicon accumulation at the interface. The composites processed at 927 °C showed formation of an interphase region of about 10–20 μm thick, as well as excellent interfacial wetting. EDS analysis gave averaged compositions of this interphase region at 74 wt % Al and 26 wt % Si, which corresponds to the composition of mullite ($3Al_2O_3 \cdot 2SiO_2$). The formation of mullite at the interface was confirmed by XRD analysis.

## 1. Introduction

Metal matrix composites (MMCs) have been developed to improve specific mechanical properties such as modulus, creep, and wear resistance of structural components. The major applications of these MMCs are aerospace parts, automobile components, and sports equipment [1–10]. The first high-strength, high-modulus fibre to be used in MMC applications was boron fibre [4]. This fibre has been used in both aluminium and titanium matrices. However, it shows limitations in the application to MMCs. For instance, boron fibres react rapidly with molten aluminium, and the mechanical properties of boron/aluminium composites degrade over the long term at high temperatures ( > 480 °C). These drawbacks have led to the development of SiC fibres [5]. There are three kinds of processing methods in fabricating SiC fibres: (1) chemical vapour deposition (CVD) of SiC on tungsten or carbon filaments [11–14], (2) diffusion-based sol–gel methods of metal alkoxides [15–17], and (3) pyrolysis of cured polymer fibres [18–20]. Owing to good bonding between SiC fibres and reactive metals and the small loss of strength degradation during high-temperature processing, SiC fibre-reinforced metal matrix composites have become viable engineering materials.

Alumina fibre is another ceramic fibre which is widely used for reinforcing metal matrices such as aluminium and magnesium [6]. Alumina fibres have been produced via slurry processing of ceramic powders and organic polymer mixtures [21–23]. Alumina fibre-reinforced MMCs are important for weight-sensitive applications operating at elevated temperatures. The chemical and oxidation resistance of alumina can overcome fibre degradation during both composite fabrication and use. Because strength and stiffness remain high at elevated temperatures, the composites creep less and have significantly better fatigue resistance than the unreinforced metals. The hardness of alumina accounts for the exceptionally good wear properties of their MMCs. Toyota Corporation Company introduced the first commercial application of an alumina fibre-reinforced aluminium composite in diesel engine pistons. This composite piston has about twice the wear and seizure resistance of the steel piston, as well as lower weight.

Inspite of these excellent properties of ceramic fibres as reinforcements for metals such as aluminium, titanium, and magnesium, they have only limited use owing to their high cost which is related to their production processes.

The inviscid melt-spinning (IMS) process has been successfully applied to fibre production using low-viscosity melts of inorganic materials such as ceramics and metals [24–30]. Furthermore, the IMS process gives a very rapid production rate of fibres and thus considerably reduces fibre cost. The formation of a stabilizing sheath on the surface of an inviscid molten stream by introduction of a reactive gas such as propane, can prevent the Rayleigh break-up and stabilize the molten stream until solidification occurs. Calcia–alumina fibre (CA) was the first ceramic fibre

* Author to whom all correspondence should be addressed.

0022–2461 

spun by IMS. Various compositions of CA were spun into fibres [26–28]. The fibres for this study have a eutectic composition of 46.5 wt % CaO and 53.5 wt % $Al_2O_3$. This fibre would be suitable for reinforcing metal matrices because it can retain about 80% strength up to approximately 800 °C. X-ray diffraction (XRD) patterns show non-crystallinity in the as-spun IMS CA fibre [31]. The properties of this amorphous IMS CA fibre are listed in Table I [32, 33]. Aluminium alloys containing high percentages of silicon (12 wt %) were selected as matrix materials for the IMS CA fibre for the following reasons: (1) to enhance the wettability of the aluminium matrix to CA fibre; it has been known that alloying elements such as magnesium, copper, lithium, silicon and nickel, which have a tendency to be absorbed in the interface and/or form an interfacial compound at the interface, can enhance wetting at the interfacial zone [34–40]; (2) to try to transform some portion of the amorphous CA fibre to a mullite ($3Al_2O_3 \cdot 2SiO_2$) phase using a reaction between $Al_2O_3$ in the CA fibre and silicon in the Al–Si matrix; mullite has been well known as an excellent high-temperature material which can maintain most of its strength up to ~1400 °C and shows the lowest creep rate up to ~1400 °C [41]. The alumina fibre-reinforced aluminium composites containing alloying elements such as lithium, magnesium and copper, gave compounds such as $LiAlO_2$, $MgAl_2O_4$, and $CuAl_2O_4$ at the interface [38, 39].

The objective of this study was to fabricate IMS CA fibre-reinforced Al–Si alloy composites using melt infiltration, and investigate the wetting behaviour and the interphase formation (mullite) at the interface of the composites.

## 2. Experimental procedure

A graphite mould consisting of three pieces (a top piston, a main cylinder, and a bottom plate) was designed for the CA/Al–Si composite fabrication. A high-grade graphite with low ash content (grade ECV, National Carbon, Cleveland, OH, USA) was used to reduce the wetting of the aluminium alloy melt with the graphite mould. Aluminium alloy (4032) was provided by Alcoa Technical Center (Alcoa Center, PA, USA) and contained 12.0 wt % Si as the major alloying element, and 0.96 wt % Cu and 0.05 wt % Fe as minor alloying elements. CA fibres (~200–300 μm diameter) were preloaded parallel to the mould axis and Al–Si alloy chunks were loaded at the top of the CA fibres. This mould was placed in a hot-press machine (Physical Science Laboratory, University of Wisconsin-Madison) which had a tungsten heating element and a diffusion pump for high vacuum (~$10^{-6}$ torr; 1 torr = 133.322 Pa). The weight of the top piston of the hot press was sufficient to break the $Al_2O_3$ film on the surface of the aluminium melt and obtain melt infiltration. Additional hydraulic pressure was not needed. Fig. 1 shows schematic drawings of the graphite mould and hot press used for the composite fabrication. Melt infiltration was done at two different temperatures (700 and 927 °C). The 700 °C temperature processing was intended to investigate wetting behaviour between fibre and matrix. The temperature of 927 °C, which is slightly lower than the crystallization temperature of this CA fibre (~980 °C), was used to obtain interface/interphase chemical reactions without causing a crystallization of this fibre. In a previous study, the crystallized IMS CA fibre showed degraded mechanical properties [32]. Fig. 2 shows

TABLE I Physical properties of as-spun IMS CA fibres

| Tensile strength (MPa) | Young's modulus (GPa) | Density (g cm$^{-3}$) | Fibre diameter (μm) | Glass transition temp. (°C) | Crystallization peak temp. (°C) | Activation energy for crystallization (kJ mol$^{-1}$) |
|---|---|---|---|---|---|---|
| 519 | 100 | 2.74 | 200–300 | ~850 | ~980 | ~550 |

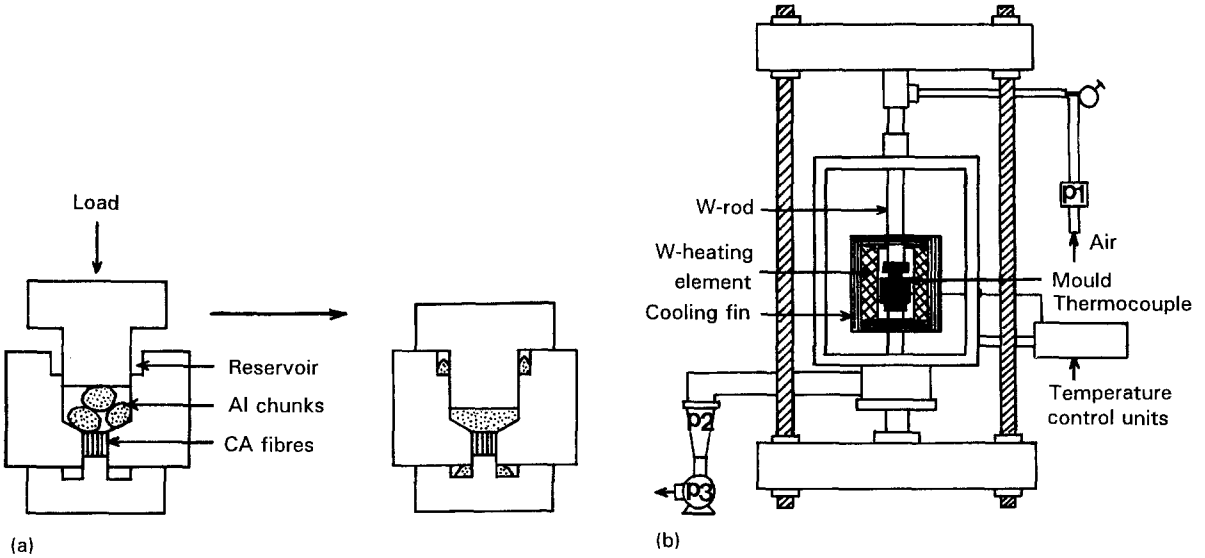


*Figure 1* Schematic drawings of (a) the graphite mould and (b) the hot press used for composite fabrications [42, 43].

the two processing schedules of (a) 700 °C and (b) 927 °C. The nipple-shaped CA/Al–Si composite was easily released from the graphite mould. For scanning electron microscopy (SEM) studies, a sample surface perpendicular to the fibre direction was polished using 400 and 600 grid SiC papers (CARBIMET, Buehler, Germany) and 1 μm $Al_2O_3$ powder (TEXMET, Buehler, Germany). A Jeol JSM 35-C SEM was used for secondary electron imaging (SEI), to investigate wetting behaviour and morphology of the interface/interphase, and backscattered electron imaging (BEI) to obtain compositional contrast at the interface region. Energy dispersive X-ray spectroscopy (EDS, Noran Co. Middleton, WI, USA) was also used with SEM analysis to provide the composition profiles across the interfacial zones of the composite. XRD (Nicolet Stoe Transmission/Bragg-Brentano, Stoe Co., Germany) with a Cu$K_\alpha$ source, a 20 s time constant, a 15°–65° scan range, and 0.02° step size, was performed for phase identification. The XRD analysis directly on the composites would not detect the new interphase formed owing to the small volume percentages ( < 5%). Some of the CA fibres could be separated from the composite by dipping the composite into a solution of sodium hydroxide (40 wt %) and distilled water (60 wt %) for about 10 min. To identify the crystalline phase on the surface of these fibres, powdered CA fibres were analysed. The resulting XRD patterns were identified using the Joint Committee on Powder Diffraction Standards (JCPDS) card to confirm the formation of mullite ($3Al_2O_3 \cdot 2SiO_2$). A list of peak positions and intensities of mullite phase, as given in the JCPDS card (15-776), is given in Table II.

TABLE II X-ray diffraction patterns for mullite ($3Al_2O_3 \cdot 2SiO_2$)

| Peak | Intensity | *d*-spacing (nm) | 2θ (deg) |
|---|---|---|---|
| 1 | 100 | 0.339 | 26.27 |
| 2 | 95 | 0.343 | 25.95 |
| 3 | 60 | 0.221 | 40.79 |
| 4 | 50 | 0.2542 | 35.28 |
| | | 0.539 | 16.43 |
| 5 | 40 | 0.2694 | 33.23 |
| 6 | 35 | 0.15242 | 60.71 |
| 7 | 25 | 0.2121 | 42.59 |
| 8 | 20 | 0.1600 | 57.56 |
| | | 0.2886 | 30.96 |
| 9 | 18 | 0.14421 | 64.57 |
| 10 | 14 | 0.17001 | 53.88 |
| | | 0.2428 | 36.99 |

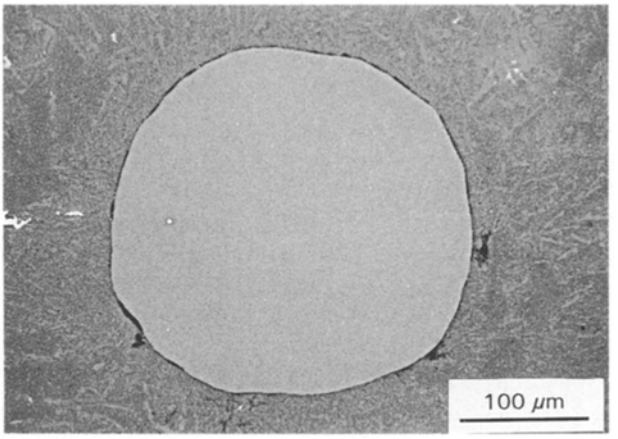


*Figure 3* The SEM back-scattered electron image (BEI) of IMS CA fibre-reinforced Al–Si alloy composite processed at 700 °C for 2 h.

## 3. Results and discussion

### 3.1. Processing at 700 °C

Fig. 3 shows the BEI of CA/Al–Si composite processed at 700 °C. Good wetting is observed at the interface of the composite, whereas in a previous study, the same CA fibre introduced into a pure aluminium matrix did not show good interfacial wetting [42, 43]. This can be explained as follows.

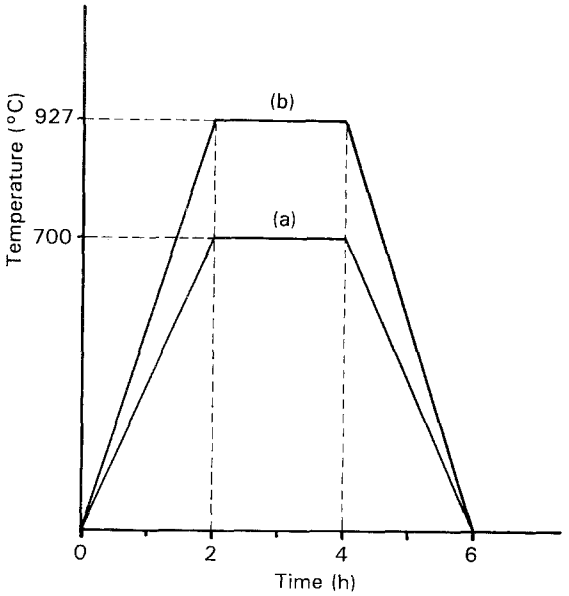


*Figure 2* The processing schedules of (a) 700 °C and (b) 927 °C for composite fabrications.

The work of spreading can be expressed by the following equation

$$W^s = \gamma^s - \gamma^l - \gamma^{sl} \quad (1)$$

where $\gamma^s$ and $\gamma^l$ are the surface tensions of solid and liquid, and $\gamma^{sl}$ is the interfacial tension between solid and liquid [43]. In the present study, the surface tension of CA fibre, $\gamma^s$, is constant. Therefore, decreased values of the $\gamma^l$ and/or $\gamma^{sl}$ can increase the work of spreading, resulting in better wettability between the fibre and liquid metal [34].

The surface tension of binary aluminium alloys in the liquid state can be given by the Gibbs' adsorption equation

$$d\gamma^l = -\Gamma_B \, d\mu_B \quad (2)$$

where $\Gamma_B$ is the excess solute concentration absorbed on the surface and $\mu_B$ is the chemical potential of the solute in the liquid. Because the chemical potential, $\mu_B$, of solute B in the mixture is given as $\mu_B = \mu_B^\circ + RT \ln a_B$ where $\mu_B^\circ$ is the chemical potential of pure B and $a_B$ is the activity of solute B in the mixture, the

following equation can be applied

$$d\mu_B = RT\,d(\ln a_B) \quad (3)$$

Combining Equations 2 and 3 gives

$$d\gamma^l = -RT\Gamma_B\,d(\ln a_B) \quad (4)$$

It is obvious that when either the excess solute concentration, $\Gamma_B$, at the surface or the activity of the solute, $a_B$, is increased, the surface energy of the aluminium melt, $\gamma^l$, is reduced. This reduced $\gamma^l$ would increase the work of spreading, $W^s$, in Equation 1, resulting in better wettability.

A compound formation at the interface can also decrease the interfacial tension between a solid and liquid $\gamma^{sl}$, leading to increased $W^s$ in Equation 1 and thus wettability.

However, a new phase formation at the interface was not found by either SEI or BEI. EDS analysis on these composites revealed large silicon accumulations ($\sim$30 wt %) at the interface regions which evidently lowered $\gamma^l$ and caused good interfacial wetting.

## 3.2. Processing at 927 °C

Fig. 4 shows the SEI and BEI of CA/Al–Si composite processed at 927 °C. A new interphase, about 10–20 μm thick, as well as an excellent wetting, was observed at the fibre–matrix interfacial zone. Evidently, for 927 °C processing, the work of spreading, $W^s$, is increased due to the decreased surface tension of the liquid, $\gamma^l$, caused by silicon accumulation at the interface, and the decreased interfacial tension between solid and liquid, $\gamma^{sl}$, caused by compound formation at the interface. Therefore, the CA/Al–Si composite produced at 927 °C should show better wetting than the composite processed at 700 °C. This was confirmed by carefully comparing the scanning electron micrographs of these composites (Figs 3 and 4). Furthermore, it was observed that the interphase was formed inside the CA fibre. This implies that matrix elements diffused into the original boundaries of the CA fibres to form the new phase. BEI of this composite showed that the interphase was depleted of the high atomic number element (calcium) because the interphase region is darker than the CA fibre area. Fig. 5 shows the blown-up image of the interphase (a) shown in Fig. 4 and a compositional scan for the corresponding interphase (b). The interphase is a polycrystalline compound with an approximately 1 μm grain size. The EDS for the composite shows a high silicon content and calcium depletion in the interphase. The amount of calcium in the interphase region was negligible. The averaged amount of aluminium and silicon in the interphase was 74 and 26 wt %, respectively, possibly indicating the formation

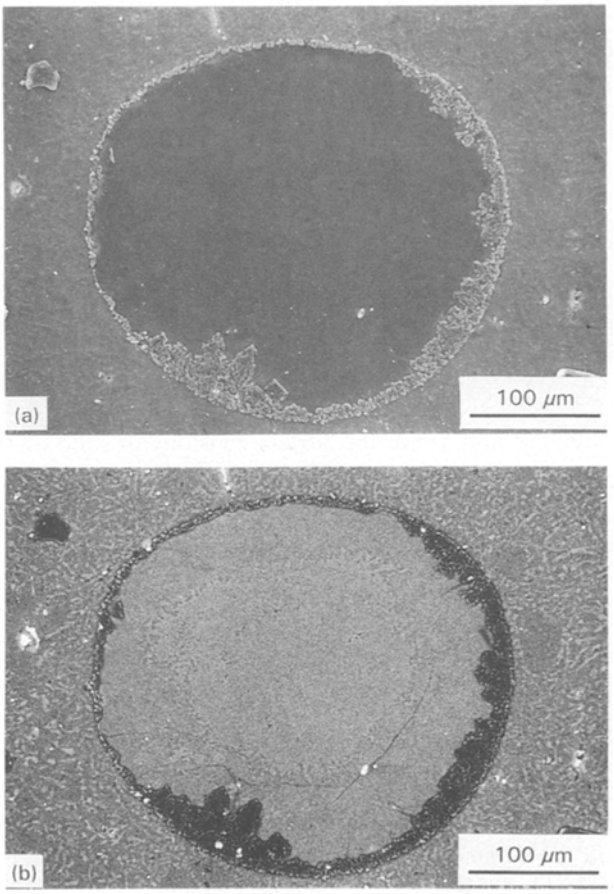


*Figure 4* (a) The SEM secondary electron image (SEI) and (b) the back-scattered electron image (BEI) of IMS CA fibre-reinforced Al–Si alloy composite processed at 927 °C for 2 h.

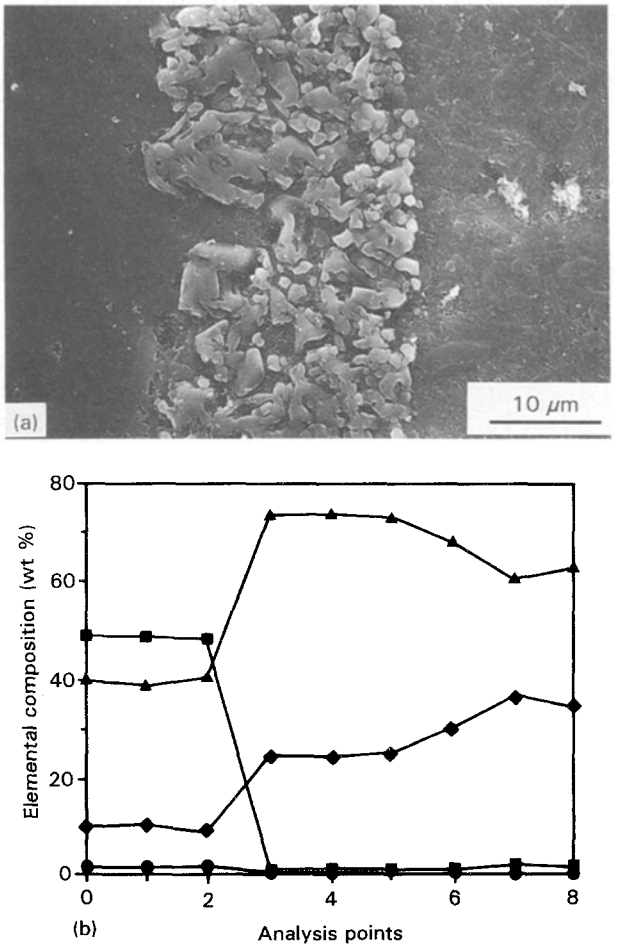


*Figure 5* (a) The blown-up SEM secondary electron image (SEI) of the interface of IMS CA fibre-reinforced Al–Si alloy composite processed at 927 °C for 2 h and (b) the compositional scan for the corresponding interface; (■) Ca, (▲) Al, (◆) Si, (●) Cu.

of mullite ($3Al_2O_3 \cdot 2SiO_2$). Silicon accumulation (~35 wt %) was also observed at the interface.

XRD was performed on the powdered CA fibres separated from both composites. Fig. 6a shows the XRD pattern for the powdered CA fibre separated from the composite processed at 700 °C. Only the broad background from amorphous CA fibre is shown. No new phase formation was detected. Fig. 6b shows the XRD pattern for the powdered CA fibre separated from the Al–Si composite processed at 927 °C. The broad background again comes from the vitreous CA fibre. The peaks (0.340(1), 0.343(20), 0.221(3), 0.255(4), 0.539(4), 0.270(5), 0.153(6), 0.212(7), 0.1604(8), 0.290(8), 0.144(9), 0.170(10), and 0.243 (10)) of mullite were identified by comparing the data in Table II. The formation mechanism of mullite at the interface of the composite can be expressed as [44, 45]

$$Si + O_2 \rightarrow SiO_2$$

$$\Delta G^\circ = -165 \text{ kcal at } 927\,^\circ\text{C} \quad (5)$$

$$3Al_2O_3 + 2SiO_2 \rightarrow 3Al_2O_3 \cdot 2SiO_2$$

$$\Delta G^\circ = -1260 \text{ kcal at } 927\,^\circ\text{C} \quad (6)$$

This implies that silicon in the Al–Si matrix is first oxidized to $SiO_2$ even at the high vacuum atmosphere and the $SiO_2$ at the interface region reacted with $Al_2O_3$ in the CA fibre to form the mullite phase. The oxygen partial pressure to obtain silicon oxidation reaction at 927 °C is only $6.93 \times 10^{-31}$ atm. Thus, even the high vacuum ($\sim 10^{-6}$ torr: $1.3 \times 10^{-9}$ atm) of the hot press has a high enough oxygen partial pressure to oxidize silicon to $SiO_2$. The negative $\Delta G^\circ$ values for the formation of $SiO_2$ and $3Al_2O_3 \cdot 2SiO_2$ indicate that these are stable phases at 927 °C.

Although only ~15 vol % IMS CA fibres was transformed to mullite phase, this would affect the overall mechanical properties of the composite, especially the creep properties. Furthermore, if redrawn IMS CA fibres of ~10 μm diameter were used, the whole fibres would be transformed to a mullite phase during processing in this composite system. Mechanical properties of this composite system are presently being studied and will be reported later.

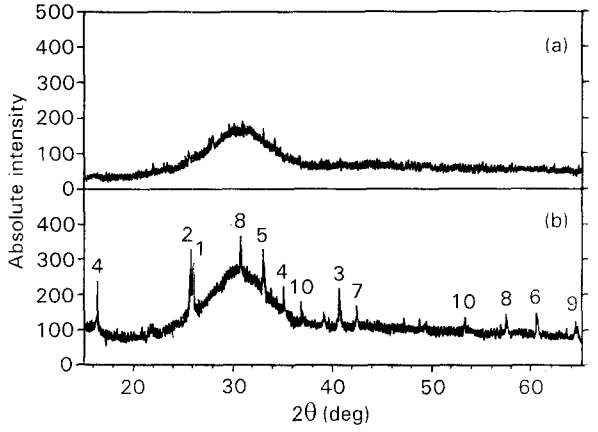


*Figure 6* The X-ray diffraction pattern for the powdered CA fibre separated from IMS CA fibre-reinforced Al–Si alloy composites processed at (a) 700 °C for 2 h and (b) 927 °C for 2 h. The numbers at the top of the peaks correspond to the peak numbers in Table II.

## 4. Conclusions

Melt-infiltration processing at 700 °C gave good interfacial wetting of the IMS CA fibre by the Al–Si alloy matrix. The alloying element, silicon, significantly accumulated at the fibre–matrix interface. For this case the good wetting was most likely due to the lowering of the surface tension of the molten alloy.

An interphase of mullite was formed between the IMS CA fibre and the Al–Si matrix for the 927 °C melt infiltration. The thickness of the mullite phase region was approximately 15 μm. Excellent interfacial wetting was observed for these composites.


## Acknowledgement

The authors wish to thank Dr Douglas A. Granger, Alcoa Technical Center (Alcoa Center, PA, USA) for kindly providing the aluminium alloys.


## References


1. J. M. ANGLIN, in "Engineered Materials Handbook", Vol. 1, "Composites" edited by T. J. Reinhart (ASM International, Metals Park, OH, 1987) p. 801.
2. T. T. SEAFANI, *ibid.*, p. 810.
3. H. B. DEXTER, *ibid.*, p. 823.
4. M. E. BUCK and R. J. SUPINKAS, *ibid.*, p. 851.
5. J. A. MCELMAN, *ibid.*, p. 858.
6. J. C. ROMINE, in "Engineered Materials Handbook", Vol. 1, "Composites" (ASM International, Metals Park, OH, 1987) p. 874.
7. D. M. ESSOCK, *ibid.*, p. 878.
8. W. C. HARRIGAN, Jr., *ibid.*, p. 889.
9. J. L. COOK and W. R. MOHN, *ibid.*, p. 896.
10. M. W. TOAZ, *ibid.*, p. 903.
11. J. O. CARLSONN, in "Encyclopedia of Materials Science and Engineering", edited by M. B. Bever (Pergamon Press, Oxford, 1986) p. 4406.
12. P. MARTINEAN, M. LAHAYE, R. PAILLER, R. NALSAN, M. COUZI and F. CRUEGE, *J. Mater. Sci.* **19** (1984) 2371.
13. S. R. NUTT and F. E. WAWNER, *ibid.* **20** (1985) 1953.
14. J. A. DICARLO, *ibid.* **21** (1986) 217.
15. K. R. VENKATACHARI, L. T. MOETI, M. D. SAKS and J. H. SIMMONS, in "Ceramic Engineering Science Proceedings", Vol. 11 edited by J. B. Wachtman (American Ceramic Society, Westerville, OH, 1990) p. 1512.
16. D. D. JOHNSON, A. R. HOLTZ and M. F. GRETHER, *ibid.*, Vol. 8 (1987) p. 744.
17. T. NISHIO and Y. FUJIKA, *J. Ceram. Soc. Jpn, Int. Ed.* **99** (1991) 638.
18. S. YAJIMA, Y. HASEGAWA, J. HAYASI and M. IMURA, *J. Mater. Sci.* **13** (1978) 2569.
19. Y. HASEGAWA, *ibid.* **24** (1989) 1177.
20. K. OKAMURA, M. SATO, T. MATSUZAWA, T. SEGUCHI and S. KAWANISHI, in "Ceramic Engineering and Science Proceedings", Vol. 9 edited by J. B. Wachtman (American Ceramic Society, Westerville, OH, 1988) p. 909.
21. F. D. BIRCHALL, in "Encyclopedia of Materials Science and Engineering". edited by M. B. Bever (Pergamon Press, Oxford, 1986) p. 2333.
22. J. D. BIRCHALL, J. A. A. BRADBURY and J. DINWOODI, in "Handbook of Composites", edited by W. Watt and B. V. Perov (North-Holland, Amsterdam, 1985) p. 115.
23. S. NOURBAKHSH, F. L. LIANG and H. MARGOLIN, *J. Mater. Sci. Lett.* **8** (1989) 1252.
24. R. E. CUNNINGHAM, L. F. RAKESTRAW and S. A. DUNN, in "Spinning Wire From Molten Metal", AIChE Symposium Series, Vol. 74, edited by J. W. Mottern and W. J. Privott (American Institute of Chemical Engineers, NY, 1978) p. 20.

25. B. S. MITCHELL, K.-Y. YON, S. A. DUNN and J. A. KOUTSKY, *Mater. Lett.* **10** (1990) 71.
26. F. T. WALLENBERGER, N. E. WESTON and S. A. DUNN, *J. Non-Cryst. Solids* **124** (1990) 116.
27. *Idem, SAMPE Q.* **9** (1990) 121.
28. F. T. WALLENBERGER, *Ceram. Bull.* **69** (1990) 1646.
29. B. S. MITCHELL, K.-Y. YON, S. A. DUNN and J. A. KOUTSKY, *Chem. Eng. Commun.* **106** (1991) 87.
30. F. T. WALLENBERGER, N. E. WESTON, K. MOTZFELT and D. G. SWARTZFAGER, *J. Am. Ceram. Soc.* **75** (1992) 629.
31. B. S. MITCHELL, K.-Y. YON, S. A. DUNN and J. A. KOUTSKY, *J. Non-Cryst. Solids* **152** (1993) 143.
32. B. S. MITCHELL, PhD thesis, University of Wisconsin, (1991).
33. Y.-M. SUNG, S. A. DUNN and J. A. KOUTSKY, *Ceram. Int.* (1994).
34. Y. KIMURA, Y. MISHIMA, S. UMEKAWA and T. SUZUKI, *J. Mater. Sci.* **19** (1984) 3107.
35. F. DELANNAY, L. FROYEN and A. DEROYTTERE, *ibid.* **22** (1987) 1.
36. T. SHINODA, H. LIU, Y. MISHIMA and T. SUZUKI, *Mater. Sci. Eng.* **A146** (1991) 91.
37. M. GUPTA, I. A. IBRAHIM, F. A. MOHAMED and E. J. LAVERNIA, *J. Mater. Sci.* **26** (1991) 6673.
38. C. G. LEVI, G. J. ABBASCHIAN and R. MEHRABIAN, *Met. Trans.* **9A** (1978) 697.
39. U. MADELENO, H. LIU, T. SHINODA, Y. MISHIMA and T. SUZUKI, *J. Mater. Sci.* **25** (1990) 3273.
40. A. MORTENSEN, *Mater. Sci. Eng.* **A135** (1991) 1.
41. I. A. AKSAY, D. M. DABBS and M. SARIKAYA, *J. Am. Ceram. Soc.* **74** (1991) 2343.
42. K.-Y. YON, PhD thesis, University of Wisconsin-Madison (1993).
43. K.-Y. YON, S. A. DUNN and J. A. KOUTSKY, *Mater. Sci. Eng.* (1994).
44. D. R. GASKELL, "Introduction to Metallurgical Thermodynamics", 2nd Edn (McGraw-Hill).
45. JANAF Thermodynamical Data, Army–Navy–Air Force Thermodynamical Panel, (The Dow Chemical Co., MI, 1962–63).

*Received 31 January*
*and accepted 13 April 1994*